AIAA JOURNAL
Vol. 38, No. 5, May 2000

Turbulent Vortex Breakdown at High Reynolds Numbers

F. Novak* and T. Sarpkaya†
Naval Postgraduate School, Monterey, California 93943

This paper deals with vortex breakdown in noncavitating swirling flows in tubes at high Reynolds numbers ($Re = U_0 D_0/\nu$ as high as 3×10^5 or $\gamma = \Gamma/\nu$ as high as 175,000). Breakdown in slender vortices of high intensity begins with a rapidly spinning spiral at a point dictated by the prevailing flow and boundary conditions. The nascent spiral bursts into turbulence shortly after its inception, i.e., the breakdowns occurring at relatively low γ or Reynolds numbers are bypassed at sufficiently high Reynolds numbers. Additional findings concern the core bifurcation, the random reversals in the sense of the spiral windings, and the absence of a reversed-flow region. The core meandering and stagnation-point darting are quantified and discussed in light of extensive velocity, turbulence, and spectrum measurements.

Introduction

VORTEX breakdown is *the transformation of a slender vortex into three-dimensional forms.* Where, how, and under what circumstances this transformation occurs in viscous vortical flows constitutes the essence of the breakdown problem. Neither a stagnation point, nor a region of reversed flow, nor the bridging of laminar-turbulent states is necessary.

The literature is abound with studies of vortex breakdown,[1–4] partly because of its intrinsic interest and partly because of its practical applications in the destruction of wing-tip vortices, in the improvement of the handling characteristics of fighter-type aircraft, and in flame stabilization in combustion. These applications involve turbulent flows at high Reynolds numbers in or about complex geometries. Even though experiments on breakdown in swirling flows in complex combustion chambers have been reported,[5] the majority of the experimental and numerical studies dealt with laminar breakdowns. In this paper we describe experiments at high Reynolds numbers and turbulent-flow conditions in a tube and vane-type apparatus similar to, but not identical to, that previously used by Sarpkaya.[1,3,6]

The difficulties experienced in describing the nature, identifying the occurrence, and predicting the characteristics of laminar vortex breakdowns in tubes and over delta wings have been reviewed most recently by Althaus et al.,[2] Sarpkaya,[3] and Visbal[4] and will not be repeated here. After 40 years of observations, measurements, and numerical experiments, the phenomenon remains largely in the qualitative, descriptive realm of knowledge. There are neither exact solutions nor universally accepted theoretical models that capture the essential physics, weave understanding into large amounts of numerical, experimental, and observational records, and offer methods of prediction. Theories based on the inviscid-flow assumptions and axial symmetry have become a rival faith to physical and numerical experiments.

Vortex breakdown in most technological applications (e.g., combustion, aerodynamics) occurs in turbulent swirling flows at high $\gamma = \Gamma/\nu$ and $Re^* = 2U_0 R_c/\nu$ [where Γ is the circulation; U_0 is a characteristic velocity (e.g., the mass-averaged axial velocity at $x = 0$, the start of the divergence of the original tube); R_c is the core radius; and ν is the kinematic viscosity], and the applicability of the information deduced from laminar flow studies to the prediction of breakdowns in turbulent flows is highly questionable. Even though there are a large number of numerical and experimental studies of swirling turbulent flows,[7] most works are dedicated either to the development of simple criteria for the identification or position of the breakdown over delta wings or to the improvement of the efficiency of combustion. None of these studies attempted to delineate the topology of the breakdown, an ingredient necessary for the understanding, numerical modeling, and the alleviation of the consequences of vortex breakdown.

Sarpkaya[3,6] was the first to show that vortex breakdown in noncavitating swirling flows in tubes at high Reynolds numbers (Re^* up to about 1.0×10^4, $\gamma \approx$ 140,000) is significantly different from the other well-known primary types (double helix, nearly axisymmetric bubble, and spiral). The present experiments have shown that at sufficiently high values of γ and Re^*, the core initiates a kink, followed by a spiral, at a point dictated by the prevailing flow and boundary conditions. The nascent spirals adjacent to the kink burst into turbulence shortly after their inception, while rotating rapidly (at about 1000 Hz). The remainder of the breakdown (beyond about the first 10–20 mm) transforms into a nominally axisymmetric cone of swirling turbulent flow, as seen in photographs taken with exposure times as small as 6 ns. The bubble and the core-recovery regions, seen in the usual path of structural transformations at low Reynolds numbers,[1] are completely bypassed at sufficiently high values of γ and Re^*.

Délery and Molton[8] examined the topology of the flow resulting from the breakdown over a delta wing at a chord-based Reynolds number of $Re = 1.46 \times 10^6$ and concluded, on the basis of their velocity measurements, that there is "a reversed flow region, of relatively small extent, which rapidly contracts and disappears, the streamwise mean velocity component becoming everywhere positive again at a short distance from the breakdown point." These experiments were confined to relatively lower γ and Re^* values, and the turbulence characteristics of the flowfield were not investigated.

The numerical studies[9–11] dealt with axisymmetric or three-dimensional laminar flows at relatively low Reynolds numbers, partly because the experimental information for comparison and code tuning was available only at comparable Reynolds numbers and partly because there has not yet been a turbulence model capable of dealing with nonisotropic turbulence in swirling flows, strongly influenced by streamline curvature and centrifugal acceleration. The available modeling approaches [direct numerical simulation, large eddy simulation, and Reynolds- or Favre-averaged Navier–Stokes equations (RANS or FANS)] have their limitations, and it is rather unlikely that standard turbulence models will help to predict the existence of large-scale structures in turbulent breakdowns observed in technologically important applications. Spall and Gatski[10] used the three-dimensional, unsteady, incompressible RANS equations in conjunction with two different turbulence models to simulate a three-dimensional turbulent breakdown at a Reynolds number of 10^4 (based on vortex core radius) in an unconfined longitudinal vortex, unimpeded by competing and complicating influences

Presented as Paper 99-0135 at the AIAA 37th Aerospace Sciences Meeting, Reno, NV, 11–14 January 1999; received 24 March 1999; revision received 19 August 1999; accepted for publication 19 August 1999.

*Lieutenant Commander, U.S. Navy, Office of Naval Research, Division 334.
†Distinguished Professor of Mechanical Engineering. Associate Fellow AIAA.

such as combustion (i.e., Hogg and Leschziner[12]). However, the calculated flowfield was not in conformity with the observations of Sarpkaya.[3,6] More recently, Spall and Gatski[13] obtained three-dimensional and axisymmetric solutions to the RANS equations using a differential Reynolds-stress model (DRSM) and the inlet boundary conditions (complete experimental profiles for the mean flow and turbulence kinetic energy at the tube inlet) provided by Sarpkaya and Novak.[14] The DRSM was found to predict quite well the location of the onset of turbulent vortex breakdown and the existence of a small recirculation region in the slightly diverging tube used by Sarpkaya and Novak.[14] However, the two-equation models failed to predict the occurrence of breakdown, presumably because of their inability to account accurately for Reynolds-stress anisotropies.[13]

One needs archival-quality physical and numerical data and physics-based phenomenological models to sort out the dominant factors for the raison d'être of the type of vortex breakdown observed at high Reynolds and circulation numbers of technological importance. This process is somewhat complicated by the well-known fact that both the real and simulated breakdowns are highly sensitive to all boundary conditions (not just the upstream conditions). It is, therefore, of paramount importance that the position of the breakdown be rendered as insensitive as possible to boundary conditions through the use of judiciously selected tube geometries and diffuser insets. This, in turn, requires a clear demonstration of the fact that the results are not specific to a single geometry and the means of fixing the location of the breakdown did not alter the physics of the phenomenon and the characteristics of the flowfield.

Experimental Apparatus and Procedure

The original experimental equipment consisted of a Plexiglas® water tank, 32 adjustable swirl vanes, a slightly diverging pipe, a constant head tank, a rotameter, and the necessary piping system. Its characteristics have been described in some detail by Sarpkaya.[1,3,6] For the present experiments the small constant head tank was replaced by centrifugal pumps of 1–10 hp to achieve the desired Reynolds numbers. It circulated the water between the apparatus and a 15-m^3 reservoir. The tube and vane assembly was placed in a 127.6-cm-long, 57.5-cm-diam stainless-steel chamber as shown in Fig. 1. The single flow meter was replaced by three larger meters of total capacity of about 15 l/s. There was no cavitation anywhere in the test tube at any Reynolds number reported here.

The shaded section of the pipe (in front of the four windows in Fig. 1 where the breakdown occurred) was made interchangeable so that tube sections of different wall profiles could be used to minimize core meandering and breakdown darting. As previously noted by Sarpkaya[1] and by others over the ensuing years, vortex cores meander, and the breakdowns do not normally remain stationary regardless of the quality of the control of the flow and angular momentum. They dart back and forth, with amplitudes dependent on the magnitudes of the primary controlling parameters (γ and Re^*), as well as on those beyond the capacity of the experimenter to control. As the core radius decreases with increasing γ and Re^*, the total pressure near the axis decreases to very low values and, if allowed, even give rise to cavitation, i.e., the position

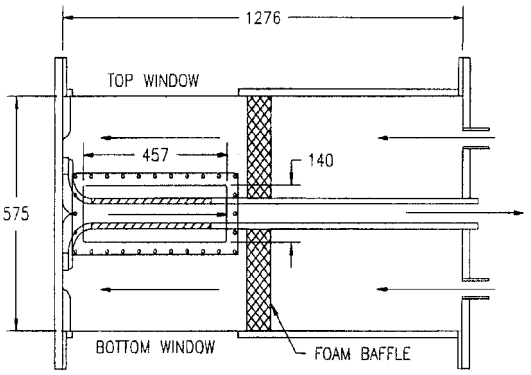

Fig. 1 Schematic drawing of the test facility (all dimensions are in millimeters).

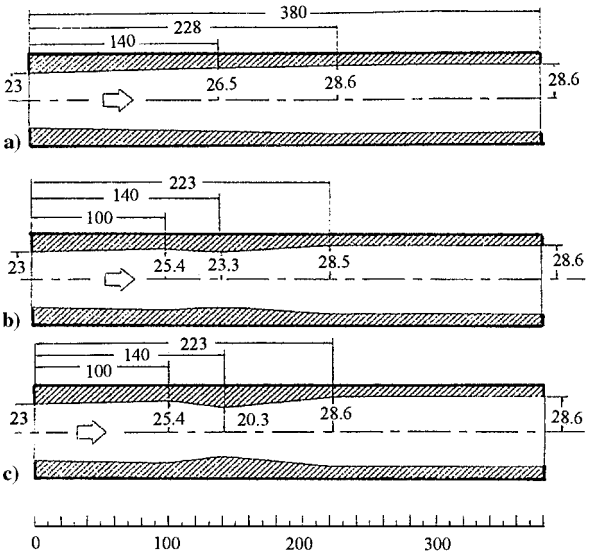

Fig. 2 Names and profiles of the test tubes used: a) h0 tube, b) h3 tube, and c) h6 tube (all dimensions are in millimeters).

of the breakdown becomes sensitized to small pressure changes in the surrounding stream. This sensitivity is aggravated, particularly in high-speed swirling flows, by the fact that a small pressure perturbation produces a much steeper rise along a streamline near the axis.[14] Unfortunately, it is not possible to describe accurately the characteristics of these low-frequency axial oscillations. Their statistical description does not allow one to introduce into the numerical model the same perturbations that occur during the physical experiments. Furthermore, accurate velocity and turbulence measurements are not possible everywhere along the breakdown because of random unsteadiness superimposed on the entire flowfield. The alternative is to render the position of the breakdown as insensitive as possible to physical boundary conditions through the use of judiciously selected tube geometries and flow rates.

In the present study experiments were first conducted with the original diverging tube described in Sarpkaya,[1] and the velocity and turbulence measurements were confined to the regions sufficiently upstream and downstream of the darting stagnation point. Subsequently, three slightly different diffuser insets were used (Fig. 2). Each inset had a gentle 1.4-deg divergence for the first 100 mm but varied shapes after that. One continued to diverge at 1.4 deg until the final diameter was reached (original tube), but the other two converged to a gentle throat located 140 mm from the entrance, and then diverged to their final diameter (about 225 mm), blending smoothly into the existing pipe. The narrowest section of the inset was carefully rounded. The inset rendered the breakdown position practically insensitive to boundary conditions and to unknown or unknowable disturbances. Data were obtained with different test tubes and flow rates. In each case the vane angle was adjusted until the circulation was sufficient for the breakdown to occur at 130–140 mm from the pipe inlet, but weak enough to avoid the formation of cavitation at the tube axis.

Throughout the experiments care was taken to minimize system-induced fluctuations. A foam baffle in the chamber (Fig. 1) damped large-scale unsteadiness, and another prevented sloshing in the external reservoir to maintain constant pump head. A Helmholtz resonator damped pressure fluctuations in the chamber. System cleanliness also was carefully maintained. Before and after experiments the water was filtered through a bypass line with a 10-μ filter. Periodically, the test tubes, windows, vanes, and bellmouth were carefully polished.

The mean velocities and turbulence intensities were measured in forward-scattering mode (in 0.1-ms coincidence window) with a three-component laser Doppler anemometer (Dantec; three-dimensional laser Doppler velocimetry with a beam separation of 38 mm, a focal length of 500 mm, and a total angle of 24 deg between the heads), a 10-W Innova Coherent laser, a three-dimensional computer-driven traversing system (with a resolution of 0.02 mm)

for the laser probes, and the forward-scatter receiving optics (with a 100-μm aperture), mounted on a manual three-dimensional traverse. Bragg-cells were used to shift the frequency of one beam of each pair by 40 MHz to provide directional sensitivity and to prevent fringe bias. The crossing of the six beams was achieved using a 50-μm pin hole and the built-in beam steerers. The probe volume (approximately 0.1 mm in diameter and about 0.8 mm in length) was positioned at the required location by use of the remotely driven x-y-z traversing unit. Even though no artificial seeding was used for a number of reasons, including the cleanliness of the tube walls and windows, the data rate almost invariably remained in excess of 1 kHz, even when the laser power and the photomultiplier gain were kept intentionally low.

No data were collected during the startup period (at least 1 h) of the operation of the system during which the count rate of bursts in coincidence mode reached at least 1000, with a validation rate of 95–99%. The number of bursts collected at a particular data station and the spatial increment between adjacent points were decided on the basis of the character of the flow measured and the objective of the measurement (velocity or spectra). The experiments were conducted in such a way that the upstream conditions at various sections were determined with the greatest precision possible, and the downstream conditions were investigated sufficiently to elucidate the important and interesting features. As such, the number of bursts and the linear density of the data stations were highest in the core region, upstream of the breakdown. Here, where the velocity gradients are steepest, 30,000 bursts were collected at each station, and the spacing was about 0.2 mm. Upstream of the breakdown, but outside the core, the gradients are nearly zero (except near the pipe wall). In this region 10,000 bursts were collected, and the spacing was 1 mm. Farther down the tube in the wake of the breakdown, 20,000 bursts were collected, and the spacing gradually became wider. For example, about 20 mm downstream of the stagnation region, the spacing was about 0.5 mm. When the purpose of measurements was the determination of the turbulence spectra, the laser Doppler velocimetry (LDV) settings such as the laser power and photomultiplier gain and voltage were adjusted to achieve higher data rates. Typically, the data rate was 1.5 kHz or higher. Also, a much larger number of bursts, in most cases at least 10^6, was collected.

Some features of the flow were measured using a Thermo-Systems, Inc. (TSI), digital particle image velocimetry (DPIV) system, comprised of two YAG lasers pulsing at 14.7 Hz. Other components consisted of optical lenses to spread the laser beam into a sheet, a 1000 × 1000 pixel digital PIVCAM (Kodak, Inc.), a synchronizer, and TSI Insight software and computer. Hollow glass beads with a specific gravity of 1.05 to 1.15, and a particle diameter of 6–12 μm were used. Velocities were computed using the Whitaker algorithm and the cross correlation between the adjacent frames, obtained in the frame straddle mode. The data rate for the pairs of frames is limited to 15 Hz, and, thus, the low-frame-capture rate remains an inherent limitation of the DPIV system.

The flow visualization was made through the use of TIO_2 (Titanium dioxide) particles, food coloring, and fluorescent dyes with high Schmidt numbers. A thin monochromatic laser light sheet (about 250 mm wide and 250 μm thick, with a wavelength of 532 nm) was provided by a Nd-YAG laser (part of a DPIV system) with a pulse duration of 6 ns. The images were recorded in digital form through the use of either a Redlake Imaging Motion Scope or a Kodak Ektapro high-speed-video system. From time to time, the said video systems were used in combination with a suitable backlighting at shutter speeds of 1/10,000 and 1/80,000 s to check the effects of the exposure time. Neither system, at their shortest exposure times, provided images as clear as those obtained through the use of the laser-light sheet provided by the Nd–YAG laser, with a 6-ns exposure time. After being recorded, the Motionscope system footage can be previewed at various playback frame rates on the monitor. For archival purposes the footage was played back at 30 fps and recorded on SVHS tape.

Results and Discussion

Evolution of Physical Events

We will present first the visual observations and photographic recordings of the breakdown and then the representative velocity, turbulence, and spectrum data for representative values of γ, Re, and Re^* (see Table 1), where the characteristic velocity U_0 in Re and Re^* is chosen as the mass-averaged axial velocity at $x = 0$ (the start of the divergence of the original tube).

Table 1 Characteristic parameters of the flows studied in the present work

$Re = [U_0(2R_0)/\nu]$	$Re^* = [U_0(2R_c)/\nu]$	$\gamma = \Gamma/\nu$	Tube	LDV mode
7.2×10^4	6720	50,000	h0	Back
1.2×10^5	6000	77,000	h0	Back
1.2×10^5	7400	80,000	h6	Forward
2.3×10^5	1×10^4	140,000	h6	Forward
2.3×10^5	1.08×10^4	140,000	h3	Forward
3.0×10^5	1.06×10^4	175,000	h3	Forward

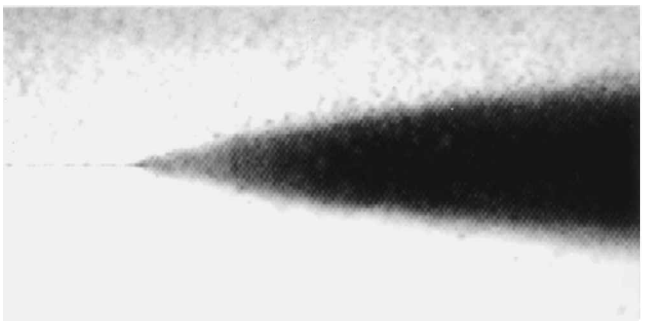

Fig. 3 Conical vortex breakdown at $Re = 1.0 \times 10^5$ as seen with a video system at 30 fps.

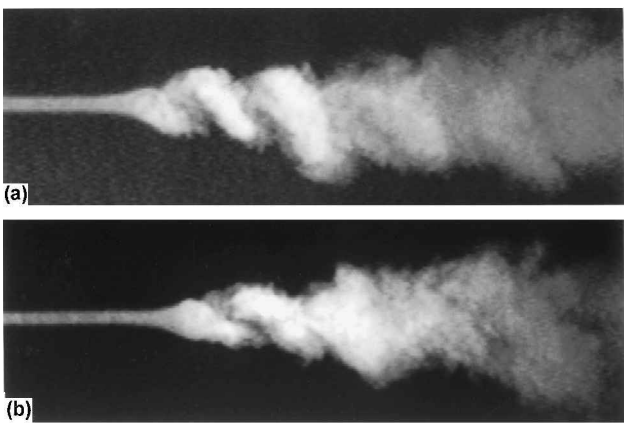

Fig. 4 Conical/spiral vortex breakdowns at $Re = 1.2 \times 10^5$. The exposure time = 6 ns (scale: 5 mm in figure = 1 mm in reality).

In describing his previous observations, Sarpkaya[6] noted that when the Reynolds number was set at $Re = 1.0 \times 10^5$ the entire breakdown resembled a cone, as in Fig. 3, growing almost linearly with distance downstream from a virtual origin. This and other photographs were made from a regular video recording, using a videographic copier. For $Re = 1.0 \times 10^5$, they showed a small, bubble-like structure in the immediate vicinity of the stagnation point. The downstream end of the bubble joined the rest of the wake in a very short distance. This and other photographs naturally gave rise to a number of important questions: Could the conical shape originate from a rapidly precessing spiral breakdown? Is there always a reverse-flow region? Could a much smaller exposure time clarify the internal structure of the flow? These and a number of other questions required video recordings at extremely small times, to capture the temporal evolution of the internal structures of the flow, and the detailed measurement of velocity and turbulence using DPIV and a three-dimensional LDV system.

Figures 4a and 4b show two sample photographs of the breakdown at $\gamma = 77,000$, $Re^* = 6.0 \times 10^3$, and $Re = 1.2 \times 10^5$, taken under conditions similar to those of Fig. 3. The only major difference is in their exposure times: $\frac{1}{30}$ s for Fig. 3 and 6 ns for Figs. 4a and 4b.

Other exposure times such as 1/2,000 s, 1/5,000 s, or even 1/80,000 s were not short enough to expose the flow structures near the first kink or the apparent stagnation point. Both Figs. 4a and 4b show that there is no bubble after the first kink. As we have foreshadowed in the Introduction, the core slightly bends and initiates either a single or a double spiral, as a result of the bifurcation of the original core, as seen in Figs. 4a and 4b. (The diameter of the dye filament upstream of the breakdown is 0.6 mm.) Almost immediately, the spirals burst into fine-scale turbulence and begin to merge with the rest of the turbulent flowfield. There are, to be sure, numerous small variations to the basic mechanism depicted by Figs. 4a and 4b. At times, a half spiral is followed by a major burst. There does not appear to be a stagnation point on the nascent spiraling core. Althaus et al.[2] noted, in connection with their Fig. 9.3.3a and b, that "the stagnation point is not located on the centerline as often assumed, but rotates around it." Visbal[4] numerically confirmed that "although there is a stagnation point associated with one of the foci, there is no stagnation point in the front of the breakdown region corresponding to the saddle in the sectional streamlines. Therefore, reverse axial flow in spiral breakdown does not imply the existence of a stagnation point in the vortex axis, as is commonly assumed."

At higher Reynolds numbers the mechanism of the structural change became even more interesting, and the breakdowns became more like axisymmetric cones. Figures 5a–5d show four examples of highly turbulent conical structures for $\gamma = 140{,}000$, $Re^* = 1.08 \times 10^4$, and $Re = 2.3 \times 10^5$. The rate of revolution at the inception of the cone is about 1000 rev/s and decreases with distance further downstream. Thus, to the naked eye or in standard speed video, the spiral structure appears as a conical wedge (Fig. 3). Had the breakdown been free from back and forth darting and other disturbances, the pure spiral form might have prevailed at all times. However, in reality, one of the several transitional forms appears occasionally. The most important of these is the bifurcation of the nascent spiral into two spirals as seen in Fig. 4a. In some instances the core gives rise to multiple windings, or trifurcate. After splitting, the filaments rotate about a common axis and after a few windings break up into turbulence. In the second transient form the individual windings become temporarily indistinguishable because of changes in the helix angle of the spiral. The final transitional forms, shown in Figs. 5a–5d, had a conical appearance even when frozen by a 6-ns exposure time. Further downstream, there were hints of a spiral-like structure within the well-mixed wedge of dye. The sense of the spiral windings changed direction from time to time, rather randomly. It was the consensus of the previous investigations that the sense of windings of the spiral is opposite to the swirling flow in tubes,

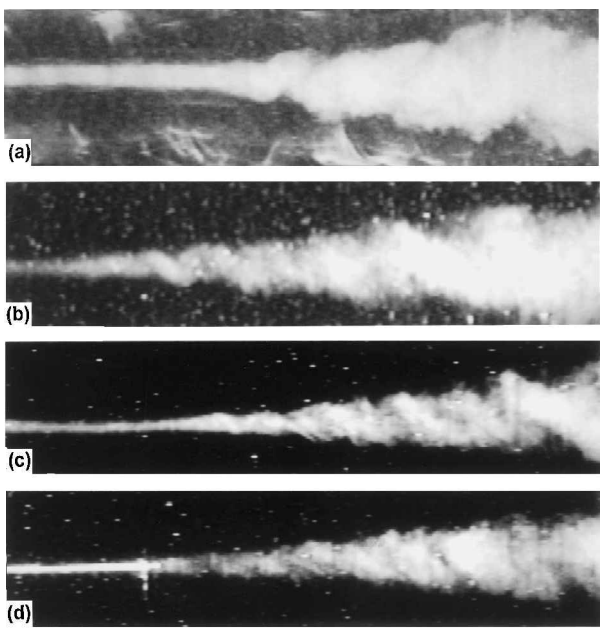

Fig. 5 Representative vortex breakdowns at $Re = 2.3 \times 10^5$. (Note the change in sense of winding in panels a and b.)

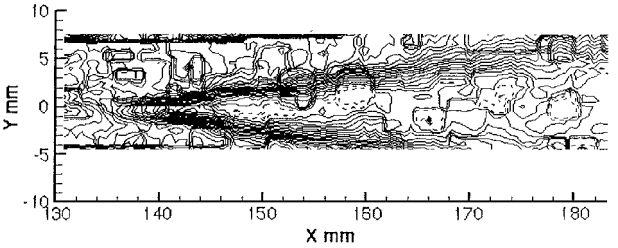

Fig. 6 Representative axial velocity contours from DPIV for $Re = 2.3 \times 10^5$.

but in the same direction with the flow over delta wings. There seemed to be a built-in bias associated with each apparatus. Now, it has been demonstrated that the bias in tubes exists only at low and intermediate Reynolds numbers (less than about 1.2×10^4).

The existence of a spiral structure in the high-Reynolds-number vortex breakdowns was confirmed through the use of numerous instantaneous axial velocity and vorticity plots, obtained through the use of a DPIV system. Here only a black and white sample of axial velocity contours is shown (Fig. 6) rather than the more exciting colored vorticity contours of dispiritingly high cost. The DPIV results were not strictly redundant with the flow visualization. When the fluorescein dye diffuses rapidly because of turbulence, the internal structure is indiscernible. The DPIV results, however, show the presence of a spiral, even 50 mm downstream of the breakdown. This is remarkable when one considers that the dye filament becomes nearly conical within, at most, 20 or 30 mm of the stagnation point. The bubble or the reverse-flow region and the core-recovery regions, seen in the usual path of structural transformations at low Reynolds numbers,[1] are completely bypassed at sufficiently high γ and Re^*. Time-averaged measuring devices such as LDV depict the spiral (at any Reynolds number) as an axisymmetric structure.

Vortex Core Meandering

In most previous experiments on vortical flows where the Reynolds number and circulation were relatively low, the amplitude of the core motion was quite inconsequential. In the present work when the Reynolds number was increased above roughly 5×10^4, the core began to move visibly about a mean centerline. Obviously, the meandering of the core complicates the interpretation of the Eulerian measurements, e.g., LDV, especially when the velocity gradients are steep. Meandering also may contaminate the turbulence measurements. For example, Westphal and Mehta[15] conducted an experiment in which a vortex was forced to oscillate (by moving the apparatus) at a low frequency and at an amplitude roughly equal to the core radius. When compared to the measurements of a vortex that was not oscillated, the Reynolds stress $\overline{u'w'}$ was 50% larger. At present, instrumentation is unable to discriminate between velocity fluctuations that are caused by unsteadiness and those that are caused by turbulence. Therefore, quantities such as turbulent kinetic energy and the Reynolds stresses will be overestimated within the immediate vicinity of the core by an amount dictated by the velocity gradients and meandering amplitudes.

A quantitative investigation of the meandering motion was carried out. The results were used to assess the effect of meandering on velocity and turbulence measurements and to devise correction schemes. Time histories of the core position, based on 1000-frames-per-second (fps) video, are shown in Figs. 7a–7c. At times the core wandered over 0.75 mm from the centerline, which is rather remarkable because the measured core radius was only about 1 mm. The core oscillated about its mean position, but neither the frequency nor the amplitude was fixed. The higher-frame-rate results have demonstrated that the rapid irregular oscillations occurred about a more slowly changing vortex position. Fourier analysis results did not reveal dominant characteristic frequencies in either the slow or the fast video results. Because the motion does display cyclic behavior, an effective amplitude of sinusoidal motion was estimated and found from visual observations to be about 0.40 mm. The histograms of both the y and z coordinates of the vortex core were well approximated by Gaussian probability density distributions. The standard deviations σ were 0.23 mm for both the lateral y and

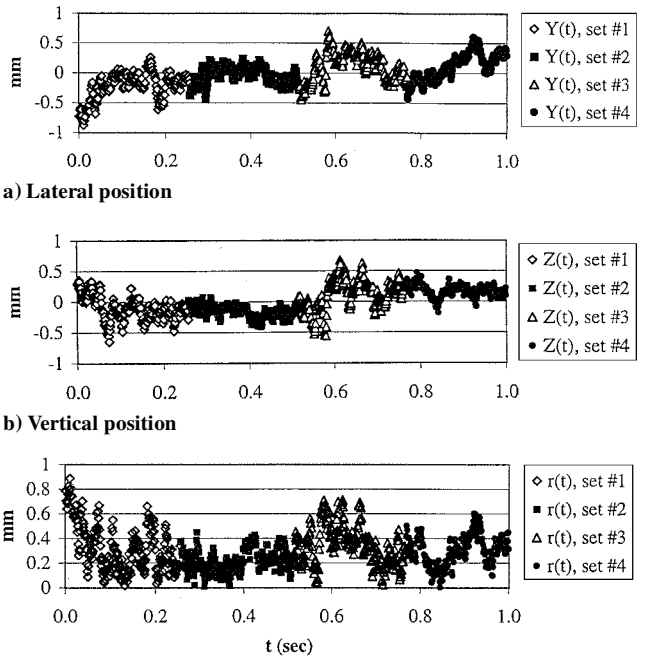

Fig. 7 Time history of vortex core position based on 1000-fps video.

vertical z positions, and 0.32 mm for the radial distance from the centerline. As expected, the most probable distance from the mean axis was nonzero, roughly 0.2 mm. This is in close agreement with the probability density function of the total radial distance from the mean centerline. This, coupled with the lack of dominant frequencies, suggests that the motion is perhaps more random than periodic.

The effect of meandering on the present results was estimated using the meandering data and a representative set of velocity profiles and the correction techniques devised by Chow et al.[16] and by Devenport et al.[17] (based on a scheme first reported by Baker et al.[18]). Both methods yielded essentially identical results.

A detailed assessment of the effect of meandering indicated that the core meandering profoundly affects the LDV results, especially the turbulence moments. Corrections to the velocity profiles with proposed methods yielded results that did not seem to be in harmony with the statistical data (histograms). The evidence suggested that the mean velocity data is more accurate than previously believed. Correction to the turbulence moments was not possible using the existing methods. Thus, the turbulence measurements within 3 core radii are not considered reliable. The primary reason for this is the relative size of the measurement volume. To achieve reliable turbulence data near the centerline of a strongly swirling and meandering flow, with or without darting, the measurement volume must be very small relative to the size of the vortex (less than about 50 μm). Currently, this is not achievable.

Stagnation Point Darting

In a high-Reynolds-number swirling flow the vortex breakdown tends to dart back and forth along the axis, compounding the matters beyond that introduced by the core meandering. Thus, even if the meandering could be eliminated completely, time-averaged Eulerian measurements will represent an average over both time and space, at least in the sections near the stagnation region. Thus, to ascertain the flowfield reliably, without excluding the stagnation point region, the darting motion needed to be accounted for or minimized. Alternatives included attempting to work around the problem through selective or intermittent measurements, or minimizing the darting motion to the maximum extent possible. The highly random nature of the motion, characterized by shorter timescales than what was found at low Reynolds number, precluded the use of intermittent measurements. The method that was deemed achievable was the suppression of the darting motion by taking advantage of the axial pressure gradient. Adverse pressure gradients promote the occurrences of breakdowns, and that favorable gradients inhibit them.[19] Even at a high Reynolds number, a tube with a converging-diverging inset might trap the breakdown in the vicinity of the throat. Such a device was used by Althaus et al.,[2] albeit at a much lower Reynolds number.

An investigation was conducted to quantify the darting motion of the vortex breakdown in the tube sections shown in Fig. 2. Time histories of the stagnation point position were recorded using the method described in connection with the core meandering. From these histograms of the breakdown location were constructed, and a Fourier analysis was carried out. As hoped, the presence of the converging-diverging section considerably reduces the darting motion. More significantly, however, the fundamental nature of the phenomenon remains unchanged. After viewing countless images from extensive high-speed video recordings of the breakdowns under wide ranges of Reynolds number and circulation in all three tubes, the conclusion was firmly made that the breakdowns are identical in all three tubes. The spiral and its variants appeared in exactly the same manner and the transition to turbulence occurred within a few windings as in the simple diverging tube. There were no distinguishing features based on a change in tube shape alone. Only the frequency of darting increased with decreasing throat size, as one might have anticipated on the basis of the stiffening of the gradients on either side of the throat. A positive outcome of the higher frequency of darting was that the LDV record length was on the order of hundreds of darting cycles, safely eliminating the possibility that the effect of the partial cycles at the beginning and end of the measurements might be nonnegligible.

Velocity and Turbulence Measurements

The LDV measurements (subjected to velocity-bias correction) were made at numerous sections along the entire length of the tubes to determine the distributions of velocities, rms values of turbulence, shear stresses, and spectra. This led to an overwhelming number of data points and plots. Here only a very small fraction of the data obtained for $\gamma = 140{,}000$ and $Re^* = 1.08 \times 10^4$, and $Re = 2.3 \times 10^5$ (using the tubes shown in Fig. 2: h0, h3, or h6) could be presented because of space limitations. For sake of consistency, this flow is described as a default state or baseline, and the others are introduced in the context of comparisons and contrasts.

The majority of the data presented here are normalized by a suitable parameter. In most cases the characteristic velocity is U_0 (the cross-sectional mean axial velocity at the tube inlet), and the length is R_0 (the tube radius at the inlet is $D_0/2$).

Experimental uncertainty, on the basis of 95% confidence, was estimated in accordance with accepted methods (e.g., Refs. 20 and 21). The summary of the extensive error analysis has shown that uncertainty for $u_{\rm rms}/U_0$, $w_{\rm rms}/U_0$, and $\overline{u'w'}/U_0^2$ are not reliable for r less than about $3R_c$. For larger values of r (in both the upstream and downstream regions), the uncertainty in $u_{\rm rms}/U_0$ and $w_{\rm rms}/U_0$ is less than 6%, but for $\overline{u'w'}/U_0^2$ is about 9%.

The measurements with $Re = 2.3 \times 10^5$ have quickly shown that there are three global regions in the breakdown topology. The first is the upstream sections, where the flow remains virtually invariant until about 10–15 mm upstream of the nominal breakdown position (at $x \approx 138$ mm). Then, a region of dramatic changes begins as the stagnation point is approached. Every feature of the flow undergoes an abrupt change within about 30–40 mm downstream of the breakdown. Finally, there is a downstream wake region where the flow relaxes, and the velocity and turbulence tend toward uniformity.

Representative axial velocities in the upstream sections, including the one very near the stagnation point, are shown in Figs. 8a and 8b. From $x = 60$ to 110 mm, the jet was quite robust, but by $x = 120$ mm deceleration began to occur. The rate of change increased with larger x and was swiftest between $x = 120$ and 130 mm. A notable characteristic of these profiles is that the collapse of the jet profile seemed to be directed outward from the centerline. At the periphery of the jet, the velocity excess persisted even while dramatic changes were occurring in the interior.

Figure 8b continues where Fig. 8a has ended and shows that the axial velocity profiles continued to change with distance along the axis, but at a more gradual pace. At $x = 140$ mm there was still

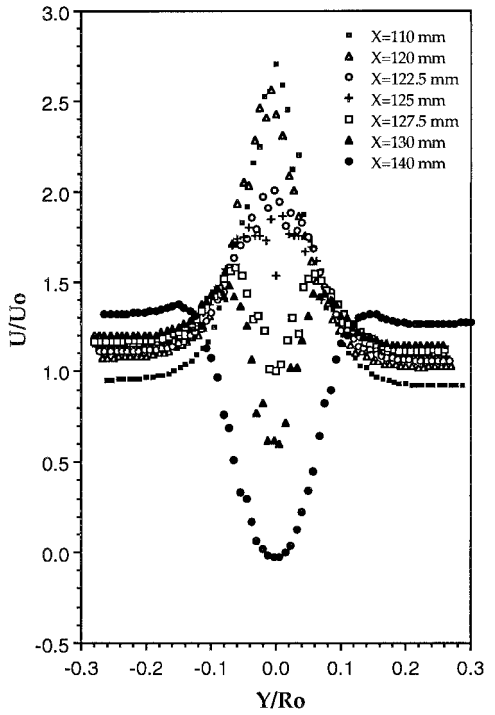

Fig. 8a U/U_0 **profiles at** $x = 140$ **mm for** $Re = 2.3 \times 10^5$.

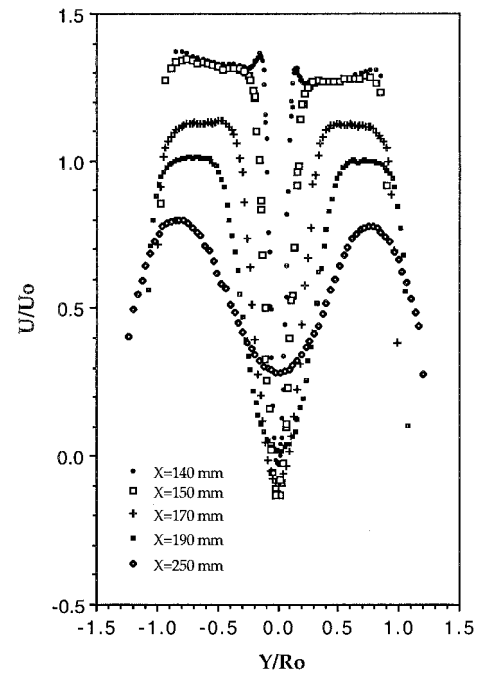

Fig. 8b U/U_0 **profiles at** $x = 140$–250 **mm for** $Re = 2.3 \times 10^5$.

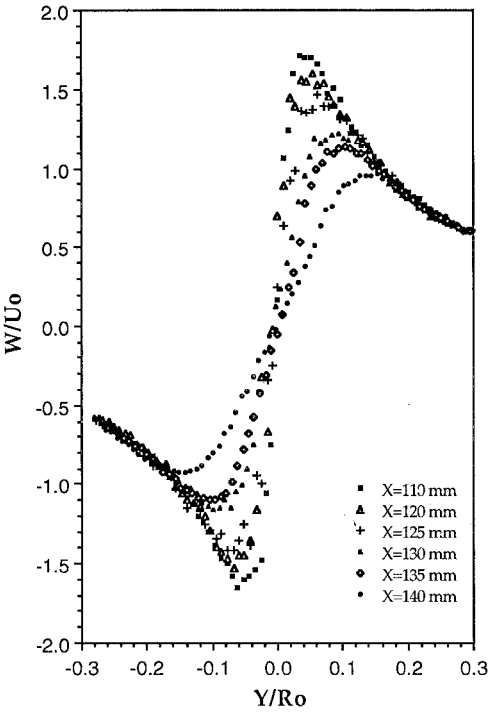

Fig. 9a U/U_0 **profiles at** $x = 110$–140 **mm for** $Re = 2.3 \times 10^5$.

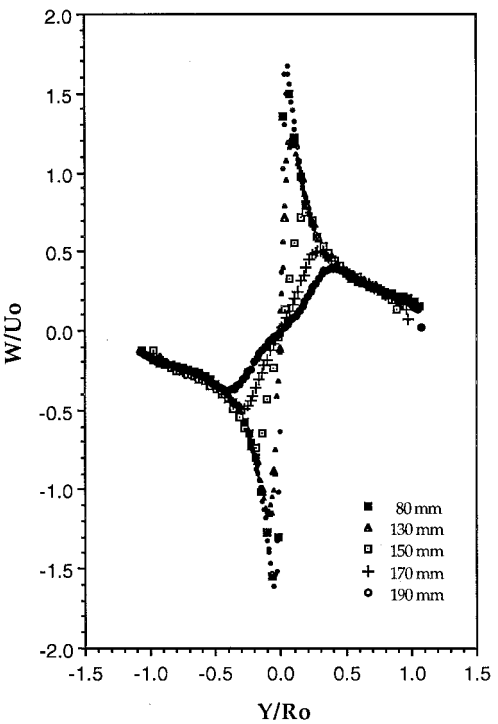

Fig. 9b U/U_0 **profiles at** $x = 80$–190 **mm for** $Re = 2.3 \times 10^5$.

evidence of a jetlike profile, but overall the plot was wakelike and the centerline velocity was slightly negative. At the next section ($x = 150$ mm) there were no longer any remnants of the jet profile. The prominent changes observed were the increasing breadth of the wake and strength of the reversed flow region. Beyond this, the wake began to relax so that the width increased but the velocity deficit decreased.

Figure 9a shows the time-averaged tangential velocity profiles in the same region that the axial velocity transformed from a jetlike to a wakelike profile. The peak velocity decreased to roughly half the magnitude found at the inlet section, and the size of the vortex core increased by a factor of 3. Figure 9b shows tangential velocity profiles selected from a wider range of axial sections, with the inlet as well as the wake regions being represented. The structure of the vortex continues to change steadily in the wake. In all, the peak tangential velocity decreased to less than one-fourth its original value, and the vortex core expanded by about 1000%. Figure 9b also demonstrates that the tangential velocity outside the core remains virtually unchanged for all axial stations, indicating that the maximum circulation is invariant, as expected.

Figure 10 shows, for various sections, tangential profiles that are normalized by the local maximum tangential velocities and core radii. The point that emerges from these profiles is that the upstream and downstream profiles are different, but self-similarity is found within each set. The profile at $x = 130$ mm, which is very near the mean stagnation point, lies between the two sets of curves. In essence, outside the viscous core the tangential velocity profile is more potentiallike in the downstream sections.

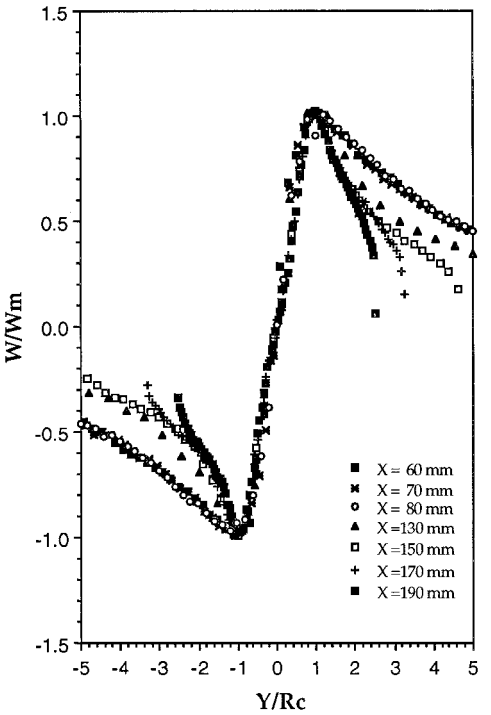

Fig. 10 W/W_m vs y/R_c at various sections for $Re = 2.3 \times 10^5$.

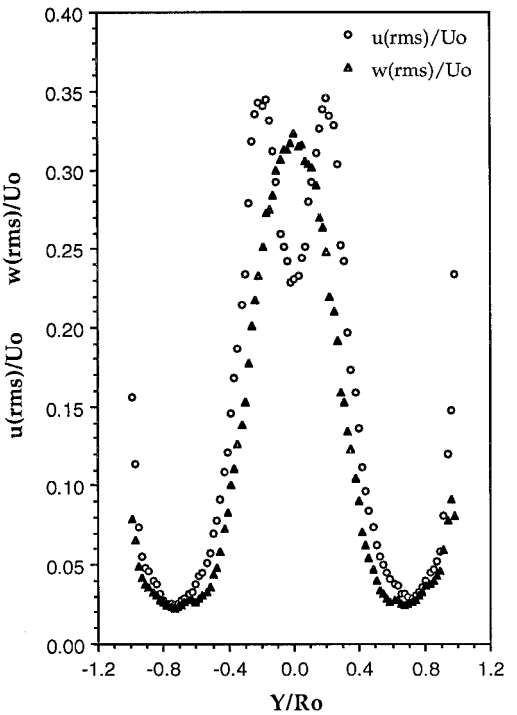

Fig. 12 u_{rms}/U_0 and w_{rms}/U_0 vs y/R_0 at $x = 170$ mm for $Re = 2.3 \times 10^5$.

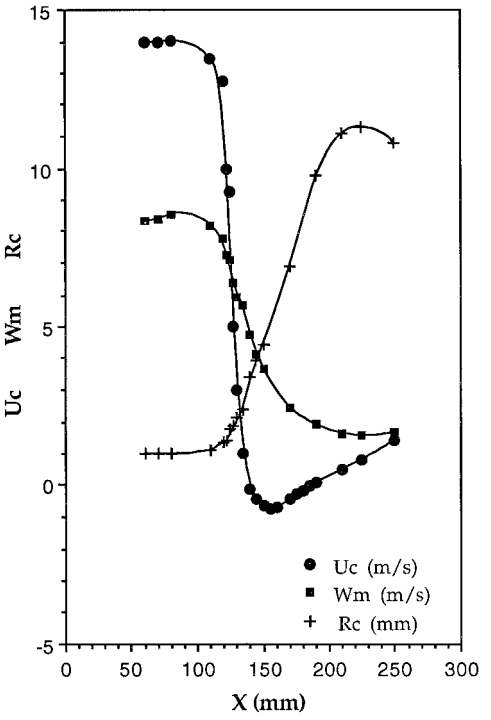

Fig. 11 Variation of U_0, W_m, and R_c with x.

Some of the foregoing can be summarized on a plot with the axial distance on the horizontal axis. Figure 11 gives the centerline axial velocity U_c, maximum tangential velocity W_m, and core-radius R_c variation along the axis. The three global regions are evident. Immediately following the inlet, there is a region where the changes to the vortex were too small to measure. This ostensibly began before the first upstream profile at $x = 60$ mm and lasted until roughly $x = 100$ mm. Then, changes commenced, and were rapid from about $x = 120$–140 mm, a span of about 20 core radii. The axial velocity decelerated from about 14 m/s to zero (30 mph to zero within 0.78 in.), and the tangential velocity decreased by a factor of 2. The core radius also abruptly began changing. Thereafter, the evolution continued but at a relatively gradual rate. The centerline axial velocity became negative at $x = 140$ mm, reached a minimum at $x = 155$ mm, and did not become positive until about $x = 190$ mm. The tangential velocity slowly evolved towards its final value of about 1.5 m/s. Throughout this region the changes to velocity seemed to be relaxing toward equilibrium. At roughly $x = 200$ mm the core radius leveled off at about 11 mm.

One representative turbulence profile at $x = 170$ mm is shown in Fig. 12. The turbulence profiles are nearly invariant in the inlet sections. As the nominal breakdown location is approached, the large data scatter clearly signals proximity to the darting stagnation point. In the wake, turbulence decays more smoothly and tends toward isotropy as seen in Fig. 12. Also, the stronger acceleration and deceleration of the axial flow in the more constricted tubes (see Fig. 2) give rise to slightly lower turbulence levels in the converging section and higher turbulence levels in the diverging sections.

Effects of Reynolds-Number Variation

The majority of the additional data are from the cases for $Re = 1.2 \times 10^5$ and 3×10^5. Numerous plots have shown that in the full range of Reynolds numbers the ratio W/U_0 exhibits only a weak dependence on Reynolds numbers. A representative axial velocity profile at $x = 150$ mm is shown in Fig. 13. As seen in Fig. 11, $x = 150$ mm is the section where the maximum reverse flow takes place for $Re = 2.3 \times 10^5$. Clearly, as the Reynolds number increases beyond 2.3×10^5, the reverse flow region begins to diminish and finally disappears at $Re = 3 \times 10^5$, i.e., there is no longer a bubble region anywhere in the flow. This is caused by the higher-level turbulence in the wake region and shows that neither a reverse flow region nor a bubble is necessary for the occurrence of breakdown, at least in high-Reynolds-number swirling flows.

Figures 14 and 15 show the axial variation of the centerline velocity and maximum tangential velocity, respectively. The mean reverse flow region vanishes as the Reynolds number approaches 3×10^5.

Profiles of $\Gamma^* = \Gamma/\Gamma_c$ (circulation normalized by circulation at the edge of the core) are shown for various Reynolds numbers in Fig. 16. As the Reynolds number is increased, the core becomes smaller, and a lower fraction of the vorticity is contained in the core, which is true in both the inlet and wake regions of the flow. However, at higher Reynolds numbers, the maximum circulation is larger, as one would expect.

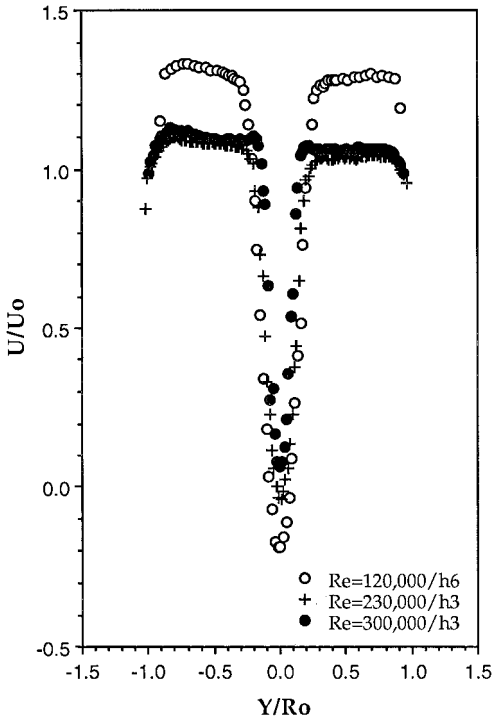

Fig. 13 U/U_0 vs y/R_0 at x = 150 mm for various Reynolds numbers.

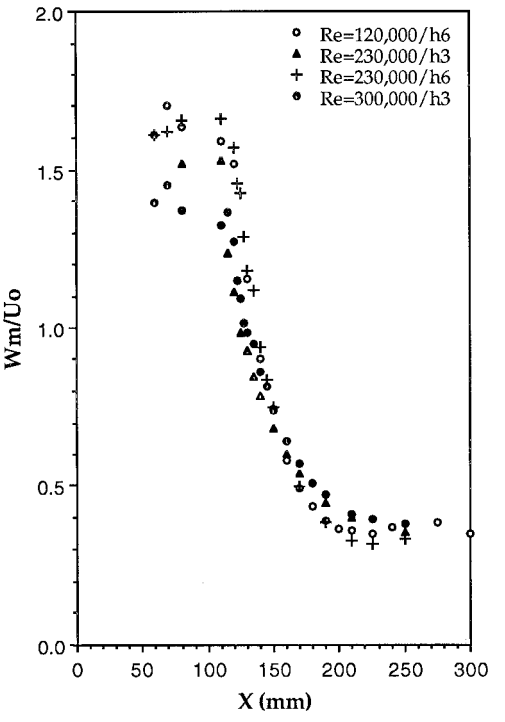

Fig. 15 Axial variation of W_m/U_0 for various Reynolds numbers.

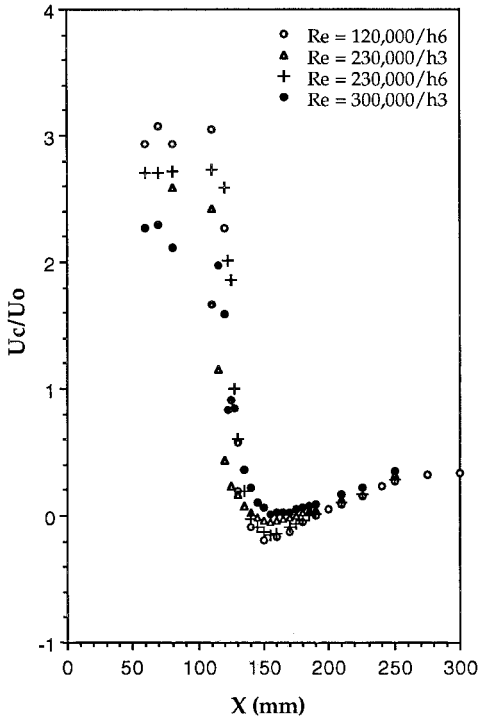

Fig. 14 Axial variation of U_c/U_0 for various Reynolds numbers.

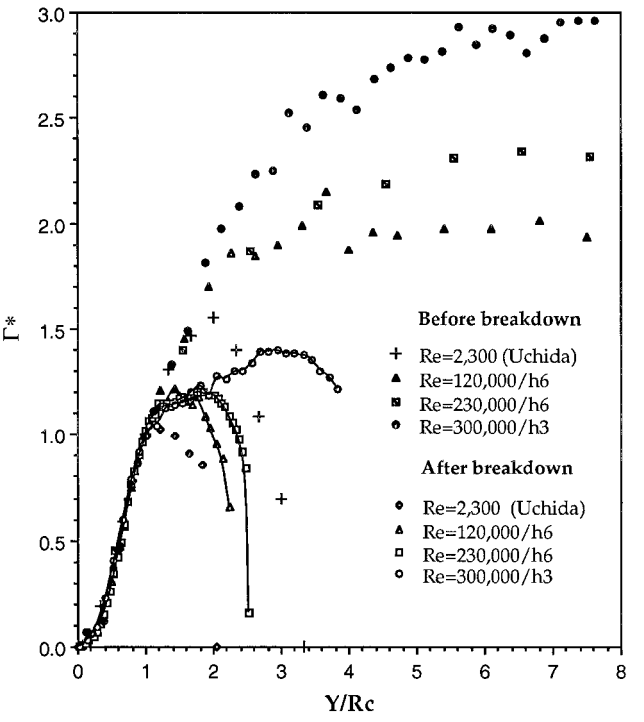

Fig. 16 $\Gamma^* = \Gamma_c/\Gamma$ profiles in various flow states.

Turbulence Spectra

For the sake of completeness, a brief presentation of the turbulence spectra will be made. As there were many common features of the results in all of the flow configurations, only the salient points will be discussed rather than examining each plot. Spectral peaks, suggestive of turbulent eddies in the flow, were observed only in the wake sections primarily because of the fact that the lower turbulence levels and axisymmetrization of the flow by the very nature of LDV measurements obscured the presence of significant energy-bearing eddies. Thus, they were relatively muted upstream, but became more conspicuous with increasing distance from the breakdown. The flat nature of the peaks gave the impression that they are broad, but, in reality, their bandwidth is approximately equal to the most energetic frequency, conforming with the descriptions of Tennekes and Lumley.[22]

Figure 17 shows the spectra for U at $x = 190$ mm for $Re = 2.3 \times 10^5$, where there are relatively well-defined peaks, at various radii, in the neighborhood of 50–60 Hz. A line corresponding to $-\frac{5}{3}$ power is drawn for each r. It is of importance in the determination of dissipation using the method that employs the curve-fitting technique in the inertial subrange of the spectral estimates (see, e.g., Ref. 23). Farther upstream, at $x = 145$ and 150 mm sections, some of the radial stations had peaks in the vicinity of 160 and 200 Hz, respectively. Although there was a clear indication of energy in

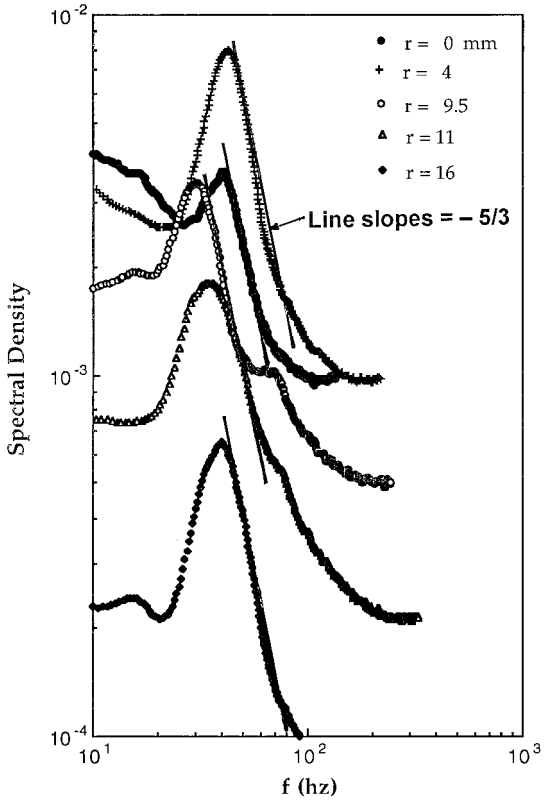

Fig. 17 Spectra of U at $x = 190$ mm for $Re = 2.3 \times 10^5$.

these frequencies, the features of the plots were less distinct than the sections further downstream. Detailed discussion of spectra and dissipation is deferred to another presentation.

Relevance to Theoretical Models

Over the past 40 years a number of theories were proposed that purported to explain or predict breakdown. Invariably, the theories that have been in existence for more than a few years have been criticized for falling short of predicting or explaining vortex breakdown. Mostly, they are based on the assumptions of laminar, inviscid, axisymmetric, and steady flow. Because this is not in agreement with the nature of the high-Reynolds-number breakdowns presented here, it seems impossible that any of these theories could capture the physics of the phenomenon.

We will dispense with the older models and take up only the most recent theoretical work by Rusak and his colleagues, which has appeared in a number of papers (see, e.g., Rusak et al.[24]). These authors have used the well-known q-vortex approximation and claimed that "the theory provides, for the first time, a consistent explanation of the physical mechanism leading to the axisymmetric vortex breakdown phenomenon in high Reynolds number flow ($Re \sim 12{,}000$) in a pipe, as well as the conditions for its occurrence." Several facts refute these claims, at least at high-Reynolds-numbers swirling flows. As typical examples, Figs. 18 and 19 show that our measurements at the inlet section do not agree with the q-vortex approximation (the relevant parameters are presented in Table 2). The flow is assumed to be inviscid and axisymmetric. Without the assumption of axisymmetry, it would have been impossible to arrive at the equations and threshold conditions described by Rusak et al.[24] Our measurements[25] and flow visualizations show irrefutably that at high Reynolds numbers the breakdown is not axisymmetric, either in the region of its inception or some distance further downstream. It is spiral, three-dimensional, and highly turbulent, and the effective viscosity is dominated by turbulent stresses. Thus, the predictions of inviscid theories can, at best, be limited to a relatively narrow range of Reynolds numbers where the breakdown exhibits reasonable axisymmetry, without bursting into turbulence over a length of several tube diameters downstream from the point of its inception. Thus, Reynolds numbers should be high enough, but not too high, to minimize the viscous effects and to avoid turbulent stresses. The theoretical models based on the assumption of inviscid axisymmetric flow have no relevance to highly turbulent high-Reynolds-number breakdowns encountered in practical applications. The numerical models need the total boundary conditions (not just those at the inlet and outlet) and a robust turbulence model that can deal with nonisotropic turbulence in swirling flows subjected to streamline curvature and strong radial pressure gradients.

Table 2 Parameters for the q-vortex representations

Re	q	U_e	$\delta = U_e / U_m$	$\omega = q\delta / U_e$
1.2×10^5/h6	1.34	5.5	2.4	0.58
2.3×10^5/h3	1.55	9.0	2.1	0.35
2.3×10^5/h6	1.68	7.3	1.8	0.40
3.0×10^5/h3	1.95	8.1	1.4	0.34

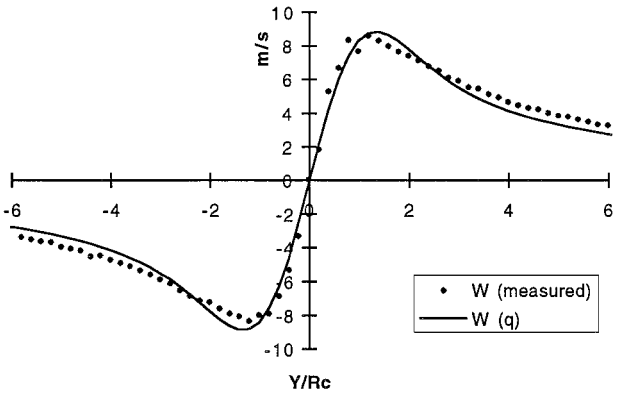

Fig. 18 Comparison of the measured and q-vortex representation of the inlet tangential-velocity profiles for $Re = 2.3 \times 10^5$/h6 (see Table 2 for the parameters characterizing the q vortex).

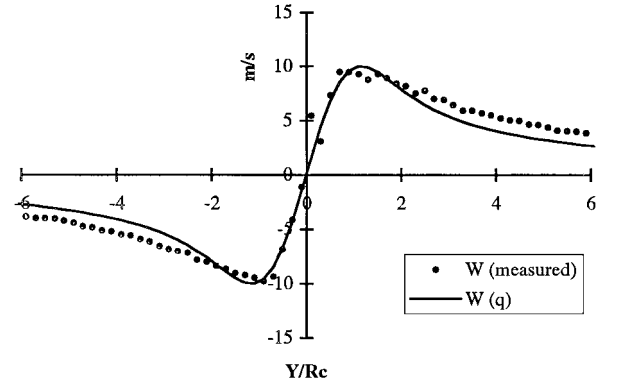

Fig. 19 Comparison of the measured and q-vortex representation of the inlet tangential-velocity profiles for $Re = 3.0 \times 10^5$/h3 (see Table 2 for the parameters characterizing the q vortex).

Conclusions

This paper described experiments on various types of vortex breakdown in *noncavitating* swirling flows at high Reynolds numbers in cylindrical tubes with or without a converging-diverging inset.

It has been shown that the vortex breakdown is the transformation of a slender vortex into three-dimensional forms. Where, how, and under what circumstances this transformation occurs in viscous vortical flows constitutes the essence of the breakdown problem. Neither a stagnation point, nor a region of reversed flow, nor the bridging of laminar-turbulent states is necessary.

The difficulties experienced in describing the nature, identifying the occurrence, and predicting the characteristics of laminar vortex breakdowns in tubes and over delta wings have been reviewed in detail. The results refute the conjectures that the circumstances of

breakdown are insensitive to the Reynolds number and the local turbulence properties. These two factors have a profound influence on the evolution of the flow. In the low-Reynolds-number regime ($Re \leq 3.5 \times 10^4$), the double helix, spiral, and bubble forms are observed. The double helix only occurs at the lower end of this regime and in a narrow range of swirl numbers γ. Also in the low-Reynolds-number regime a spiral may exist to the exclusion of other forms. Under certain conditions the spiral may periodically degenerate to a form that has a bubble-like appearance and a single recirculation cell with reversed axial flow at the centerline.

In the transitional regime ($3.5 \times 10^4 \leq Re \leq 1.0 \times 10^5$) the two-celled type of bubble continues to precede the spiral. This is referred to here as the transition regime because the separation between the bubble and the spiral decreases to the extent that some mutual interference begins between the two forms. The bubble and spiral interact, but the spiral retains its form more robustly than the bubble.

In the high-Reynolds-number regime ($Re > 1.0 \times 10^5$) the spiral breakdown bypasses the two-celled bubble form. Thus, the conical breakdown is born from a few spirals that are rotating at very high speeds (about 1000 rev/s) and bursting into turbulence. An additional distinguishing feature between the high- and low-Reynolds-number breakdowns, as discerned from the LDV results, is that the mean axial velocity at the centerline never becomes negative (reversed flow) for a Reynolds number larger than about 3×10^5. Clearly, of all of the known forms, *the spiral emerges as the most fundamental breakdown form.* All other forms can be regarded as transient states affected by various types of instabilities. The nearly axisymmetric form has served to excite imagination, to test some numerical schemes, and to produce numerous explanations of the breakdown phenomenon. However, at very high values of γ and Re^*, the breakdown acquires forms and characteristics never seen before: extremely high rates of revolution, arbitrary reversals of the sense of the winding of the nascent spiral,[25] darting of the stagnation point, meandering of the core, onset of the core-bifurcation or core-trifurcation, intense nonisotropic turbulence, and a conical shape, resembling a swirling jet. Despite physical similarities in the still images, it would not be meaningful to assume that a low-Reynolds-number solution to spiral vortex breakdown would be a satisfactory simulation of the high-Reynolds-number spiral/conical turbulent vortex breakdown.

Devising a theory that predicts the occurrence, or explains the underlying mechanisms of vortex breakdown, would be a crowning achievement. However, because such a theory has proven to be elusive, it seems inevitable that physical and numerical experiments will receive ever-increasing emphasis. The presence of a rotating spiral, as opposed to an axisymmetric form, has profound implications on the connection between the data, the truth, and the theoretical idealizations. The time-averaged results do not, and cannot, depict the essence of the instantaneous breakdown flowfield, as evidenced by the DPIV results. In the mean a spiral appears as a single-celled axisymmetric structure. But, the idealized axisymmetric breakdowns bear no resemblance either in shape or in character to physically realizable vortex breakdowns at high Reynolds numbers, which are neither axisymmetric nor laminar either in the region of their inception or some distance downstream. If there is any hope of making realistic numerical simulations of turbulent vortex breakdowns, all boundary conditions (not just those at the inlet and outlet) and, in particular, the velocity and turbulence profiles and the turbulence dissipation need to be known with sufficient precision. It is clear from our measurements that q vortex is not a reasonable approximation, and the Reynolds stresses are indeed very large in the turbulent vortex breakdown, i.e., the effective viscosity is dominated by turbulent stresses. Thus, the predictions of inviscid theories can, at best, be limited to a very narrow range of Reynolds numbers (say, $5 \times 10^3 < Re < 1.2 \times 10^4$). Obviously, one cannot emphasize strongly enough the need for a robust turbulence model that can deal with nonisotropic turbulence in swirling flows subjected to streamline curvature and strong radial pressure gradients.

Acknowledgment

This research is being supported by the National Science Foundation awarded to T. Sarpkaya under Grant CTS-9612528. This support is gratefully acknowledged.

References

[1] Sarpkaya, T., "On Stationary and Traveling Vortex Breakdowns," *Journal of Fluid Mechanics*, Vol. 45, Feb. 1971, pp. 545–568.

[2] Althaus, W., Brücker, C. H., and Weimer, M., "Breakdown of Slender Vortices," *Fluid Vortices*, edited by S. Green, Kluwer Academic, Norwell, MA, 1995, Chap. 9.

[3] Sarpkaya, T., "Vortex Breakdown and Turbulence," AIAA Paper 95-0433, Jan. 1995.

[4] Visbal, M. R., "Computational and Physical Aspects of Vortex Breakdown on Delta Wings," AIAA 95-0585, Jan. 1995.

[5] Chen, R. H., Driscoll, J. F., Kelly, J., Namazian, M., and Schefer, R. W., "A Comparison of Bluff-Body and Swirl-Stabilized Flames," *Combustion Science and Technology*, Vol. 71, No. 3, 1990, pp. 197–211.

[6] Sarpkaya, T., "Turbulent Vortex Breakdown," *Physics of Fluids*, Vol. 7, No. 10, 1995, pp. 2301–2303.

[7] Rhode, D. L., Lilley, D. G., and McLaughlin, D. K., "On the Prediction of Swirling Flowfields Found in Axisymmetric Combustor Geometries," *Journal of Fluids Engineering*, Vol. 104, No. 2, 1982, pp. 378–384.

[8] Délery, J., and Molton, P., "Topology of the Flow Resulting from Vortex Breakdown over a Delta Wing at Subsonic Speed," *Acta Mechanica [Suppl]*, Vol. 4, No. 4, 1994, pp. 297–304.

[9] Krause, E., "The Solution to the Problem of Vortex Breakdown," *Lecture Notes in Physics*, Vol. 371, 1990, pp. 35–50.

[10] Spall, R. E., and Gatski, T. B., "Numerical Calculations of Three-Dimensional Turbulent Vortex Breakdown," *International Journal for Numerical Methods in Fluids*, Vol. 20, No. 4, 1995, pp. 307–318.

[11] Breuer, M., and Hänel, D., "A Dual Time-Stepping Method for 3-D Viscous Incompressible Vortex Flows," *Computers and Fluids*, Vol. 22, Nos. 4–5, 1993, pp. 467–484.

[12] Hogg, S., and Leschziner, M. A., "Computation of Highly Swirling Confined Flow with a Reynolds Stress Turbulence Model," *AIAA Journal*, Vol. 27, No. 1, 1989, pp. 57–63.

[13] Spall, R. E., and Gatski, T. B., "Turbulent Vortex Breakdown: A Numerical Study," *Dynamics of Slender Vortices*, edited by E. Krause and K. Gersten, Kluwer Academic, Norwell, MA, 1998, pp. 307–319.

[14] Hall, M. G., "A Theory for the Core of a Leading-Edge Vortex," *Journal of Fluid Mechanics*, Vol. 11, Sept. 1961, pp. 209–228.

[15] Westphal, R. V., and Mehta, R. D., "Interaction of an Oscillating Vortex with a Turbulent Boundary Layer," *Experiments in Fluids*, Vol. 7, No. 2, 1989, pp. 405–411.

[16] Chow, J. S., Zilliac, G. G., and Bradshaw, P., "Mean and Turbulence Measurements in the Near Field of a Wingtip Vortex," *AIAA Journal*, Vol. 35, No. 10, 1997, pp.1561–1567.

[17] Devenport, W. J., Rife, M. C., Liapis, S. I., and Follin, G. J., "The Structure and Development of a Wing-Tip Vortex," *Journal of Fluid Mechanics*, Vol. 312, Nov. 1996, pp. 67–106.

[18] Baker, G. R., Barker, S. J., Bofah, K. K., and Saffman, P. G., "Lazer Anenometer Measurements of Trailing Vortices in Water," *Journal of Fluid Mechanics*, Vol. 65, Aug. 1974, pp. 325–336.

[19] Sarpkaya, T., "Effect of Adverse Pressure Gradient on Vortex Breakdown," *AIAA Journal*, Vol. 12, No. 5, 1974, pp. 602–607.

[20] Moffat, R. J., "Contributions to the Theory of Single-Sample Uncertainty Analysis," *Journal of Fluids Engineering*, Vol. 104, No. 2, 1982, pp. 250–260.

[21] Kline, S. J., "The Purposes of Uncertainty Analyses," *Journal of Fluids Engineering*, Vol. 107, No. 2, 1983, pp. 109–123.

[22] Tennekes, H., and Lumley, J. L., *A First Course in Turbulence*, MIT Press, Cambridge, MA, 1972, pp. 248–287.

[23] Yadav, A. K., Raman, S., and Sharan, M., "Surface Layer Turbulence Spectra and Dissipation Rates During Low Winds in the Tropics," *Boundary-Layer Meteorology*, Vol. 79, No. 3, 1996, pp. 205–223.

[24] Rusak, Z., Wang, S., and Whiting, C. H., "Axisymmetric Breakdown of a Q-Vortex in a Pipe," AIAA Paper 97-0441, Jan. 1997.

[25] Sarpkaya, T., and Novak, F., "Turbulent Vortex Breakdown: Experiments in Tubes at High Reynolds Numbers," *Dynamics of Slender Vortices*, edited by E. Krause and K. Gersten, Kluwer Academic, Norwell, MA, 1998, pp. 287–296.

A. Plotkin
Associate Editor